Advanced Methods for Space Simulations, edited by H. Usui and Y. Omura, pp. 23–46.

Vlasov-code simulation

J. Büchner

Max-Planck-Institut für Sonnensystemforschung, 37191 Katlenburg-Lindau, Germany

Currently optimum numerical schemes which are run on modern fast CPU, large memory parallelized computer systems led to a revival of kinetic codes which directly solve the Vlasov-equation describing collective collisionless plasmas. For many years due to restricted computer resources, collisionless plasmas have been simulated mainly by re-graining the flow of the distribution functions of phase space via introducing macro-particles in a particle-in-cell (PIC) approach. The mathematical advantage in using Lagrange-Euler PIC codes is their replacement of the treatment of the advection-type partial differential Vlasov equation by the solution of ordinary differential equations of macro-particle motion. Physically PIC-codes re-coarse-grain the continuous collisionless plasma distribution function flows introducing, this way un-physically large shot-noise of the finite number macro-particles. In other words, PIC codes replace the usually huge plasma parameter $n\lambda_D^3 \approx 10^{10}$ of space plasmas by the much smaller number of particles per cell of the order of $n_m\lambda_D^3 \approx 100$, where n_m is the number density of macro-particles and the Debye length λ_D is the typical size of a simulation cell. The arising noise problem limits the applicability of PIC codes to the investigation of insensitive to fine non-linear resonant and micro-turbulent collective field-particle interaction phenomena, the small number of macro-particles does not allow to describe the acceleration of a few particles to high energies etc. Instead Vlasov codes provide a powerful tool for low noise studies of collisionless plasmas with a fine resolution of the phase space including those regions where trapping occurs or where particles move at speeds close to wave velocities. The obvious price for the noise reduction is the numerical complication. Due to the lack of a right-hand side the Vlasov-equation causes a filamentation of the distribution function into small-scale structures, which have to be treated correctly. We discuss this and other important aspects of Vlasov code simulations and demonstrate their abilities by a number of space physics applications. We argue that the total numerical effort of Vlasov codes which solve the same sensitive to noise and phase space filamentation problem does not exceed the effort necessary for a similarly accurate PIC code.

1 Introduction

Most of the plasma in space is collisionless, i.e. the plasma parameter $n\lambda_D^3$ is huge, e.g. 10^{10}. Hence collective plasma phenomena dominate over binary collisional interactions. Collective interactions are especially efficient when wavelength or spatial localization, wave frequencies or time scales become comparable with characteristic dispersion scales of the plasma as there are gyro-radii, inertial or Debye lengths, gyro- and plasma frequencies. Nonlocal and nonlinear interactions between

plasma and waves have to be described, i.e., the propagation of kinetic Alfén waves in inhomogeneous media, collisionless shocks, warm beam instabilities, collisionless ("anomalous") transport and magnetic reconnection. The physics of collisionless plasmas is well described by a self-consistent solution of a system of Vlasov- and Maxwell's equations (see Section 2). Due to its non-locality and non-linearity in many important situations no analytical solutions of the Vlasov equation can be found, i.e. numerical solutions and simulation approaches are necessary.

First attempts were made in the 1960s to numerically solve the Vlasov-equation directly, e.g. by the "waterbag" approach (see Section 3). Since than, however, most numerical simulations of collisionless plasmas have been carried out by means of Particle-In-Cell- (PIC) approaches (see, e.g., Birdsall and Langdon, 1985). The PIC-approach restores and even exaggerates the coarse-graininess of the plasma by restoring and even exaggerating the discrete character of its elements, the particles, clustering many of them into macro-particles. At least, this way one can replace the solution of the partial differential Vlasov-equation by the solution of the ordinary differential equations of motion of the macro-particles. The particle orbits are the characteristics of the Vlasov-equation. This allows a combined Lagrange-Euler method of solution: the phase space density along the trajectories is exactly conserved, i.e. one has just to upgrade charge density and currents by extrapolating them to an Eulerian (i.e. fixed in space) grid on which the electromagnetic fields are calculated by solving Maxwell's equations. PIC codes are simple, robust and scalable (see Y. Omura's chapter in this volume). Their principal weakness is the numerical strong shot-noise caused by the limited number of heavy macro-particles. The particle noise leads to numerical collisions and artificial dissipation, destroys fine resonance may trigger un-physical instabilities. The heavy macro-particles do not represent fine velocity space, e.g. acceleration effects. And, as we will show in Section 6, they are not at all less expensive numerically than direct Vlasov codes provided the parameters (mainly the number of particles per cell) are chosen to reach the same phase space resolution.

A direct solution of the Vlasov-equation is free of the (macro-) particle noise of PIC codes. Perhaps just the numerical effort due to the necessity to solve the advection-type Vlasov-equation and the filamentation of the phase space have restricted the use of Vlasov-codes for the last thirty years to the treatment of low-dimensional and electrostatic problems. Electrostatic beam instabilities were considered by electrostatic 1D1V schemes, gradient instabilities already need at least 2D schemes. For the simulation of kinetic reconnection even 3D3V codes are necessary to describe the mode coupling of this essentially three-dimensional process (Büchner, 1999). Most space physics problems are higher-dimensional and, such as the reconnection problem, even up to three-dimensional in the real, configurational space (3D) and three-dimensional in the velocity (3V) or momentum (3P) space, i.e. six-dimensional in the full phase space. The solution of the Vlasov-equation for distribution functions in a six-dimensional phase space with a resolution of, say, a hundred grid points in each dimension needs to store function values for 10^{12} grid points! High resolution multidimensional Vlasov-code simulations are, therefore, numerically very expensive. They need huge computer resources and parallel computing

mandatory as well as the choice of optimum algorithms. At the moment mainly low dimensional electrostatic or simplified Vlasov approaches like gyro-kinetic codes are used, e.g. for strong laser-plasma interactions. The utilization of higher dimensional space physical applications of Vlasov-codes are still in their infancy. At the moment no textbook exists which would cover the major aspects of Vlasov-codes and offer optimum solution schemes like Birdsall and Langdon (1985) for PIC-codes. This tutorial discusses important aspects of Vlasov simulations in order to encourage the future development and implementation of Vlasov-codes for the solution of space physics problems. We first, in Section 2 introduce the basic equations and discuss the conditions of their applicability. In Section 3 we discuss the specific problems arising when solving the Vlasov equation and review possible efficient numerical treatments. Since in the existing literature an emphasis is put on semi-Lagrangian methods, which need an extrapolation of the Lagrangian solutions on the Eulerian grid, where the fields are calculated, we discuss in more detail a contrasting finite volume discretization scheme which allows a very accurate treatment, conservative of the Vlasov equation. In Section 5 we present several applications of Vlasov codes to the solution of important space physics problems. Finally, in Section 6, after summarizing the main points to be taken care of in Vlasov simulations, we quantify the relative numerical effort of Vlasov and PIC codes, applied to solve comparable collisionless plasma problems and give an outlook toward future research directions.

2 Basic Equations

The kinetic physics of collisionless plasmas is well described by the single particle distribution function $f_j(\mathbf{r}, \mathbf{v}, t)$, solution of the Vlasov (1938) equation. The Vlasov equation is essentially a Boltzmann equation with a vanishing r.h.s., i.e. without an explicit collision term. However, most importantly, the Vlasov equation takes into account the interaction between particles via their self-generated collectively formed electromagnetic fields, which have to be consistently calculated by solving Maxwell's equation for the charge densities and currents caused by the moving plasma particles. The collective interactions dominate the binary interactions (collisions) between particles in plasmas, i the plasma parameter $n\lambda_D^3$ is large (n is the plasmas number density, $\lambda_D = \sqrt{\kappa_B T/m\omega_p^2}$ the Debye length and $\omega_p = \sqrt{ne^2/m\epsilon_o}$ the plasma frequency). Typical plasma parameters are 10^7–10^9 for fusion plasmas, in typical space situations the $n\lambda_D^3$ is even larger than 10^{10}. In this case and for times shorter than $n\lambda_D^3\omega_p^{-1}$, not only the collisions between particles but even the very existence of discrete particles is negligible. The total derivative of the distribution function, forming the left hand side of the Vlasov-equation, can be formulated either in an advection form, where the velocity (or momentum $\vec{p}$) is treated as an independent variable, e.g.

$$\frac{df_j}{dt} = \frac{\partial f_j}{\partial t} + \vec{v}\frac{\partial f_j}{\partial \vec{r}} + \frac{e_j}{m_j}\left(\vec{E} + \frac{1}{c}\vec{v} \times \vec{B}\right)\frac{\partial f_j}{\partial \vec{v}} = 0 \tag{1}$$

or in a conservative form where the velocity (or momentum $\vec{p}$) is a dependent variable. The subscript j denotes the particle species, e.g. $j = e, p$ for electrons and protons, respectively. The conservative form of the Vlasov equation expresses the conservation of the number of particles in a closed phase space volume Ω. In agreement with the Liouville theorem from the definition of the particle number (we omit the index j)

$$N = \int_\Omega f(\vec{r}, \vec{v}, t)\, d^3r d^3v = \int_\Omega f(\vec{R}, t)\, d\Omega = \text{const.}, \tag{2}$$

where $\vec{R} = \{\vec{r}, \vec{v}\}$ is the six-dimensional phase space vector, a total differentiation of Eq. (2) over time reveals

$$\frac{dN}{dt} = \int_\Omega \left\{ \frac{\partial f(\vec{R}, t)}{\partial t} + \frac{\partial f}{\partial \vec{R}} \cdot \frac{d\vec{R}}{dt} \right\} d\Omega = \int_\Omega \left(\frac{\partial f}{\partial t} + \nabla f \vec{U} \right) d\Omega = 0 \tag{3}$$

where ∇ is the six-dimensional phase-space derivative, defined as:

$$\nabla = \{\nabla_{\vec{r}}, \nabla_{\vec{v}}\} = \left\{ \frac{\partial}{\partial \vec{r}}, \frac{\partial}{\partial \vec{v}} \right\} = \frac{\partial}{\partial \vec{R}} \tag{4}$$

and $\vec{U}$ is the six-dimensional phase space flow vector defined as the total time derivative of $\vec{R}$:

$$\vec{U} = \left\{ \vec{U}_{\vec{r}}, \vec{U}_{\vec{v}} \right\} = \frac{d\vec{R}}{dt} = \left\{ \dot{\vec{r}}, \dot{\vec{v}} \right\} = \left\{ \vec{v}, \frac{\vec{F}}{m} \right\} \tag{5}$$

For the second term in the integrals (3) the Gauss theorem gives:

$$\int_\Omega \nabla f \vec{U} d\Omega = \oint_{S(\Omega)} f\, (\vec{n} \cdot \vec{U}) dS \tag{6}$$

where $S(\Omega)$ is the surface of the phase space volume and $\vec{n}$ its normal direction. Using expression (5) one obtains the integral form of the conservative Vlasov Eq. (3)

$$\frac{\partial N}{\partial t} = \frac{\partial}{\partial t} \int_\Omega f d\Omega = \int_\Omega \frac{\partial f}{\partial t} d\Omega = -\oint_{S(\Omega)} f\, (\vec{n} \cdot \vec{U}) dS \tag{7}$$

Equation (7) means that the rate of change of the number of particles inside a domain Ω equals the integral flux of f through the surface of the domain $S(\Omega)$. From expression (4) one also obtains the differential form of the conservative Vlasov equation

$$\frac{df_j}{dt} = \frac{\partial f}{\partial t} + \nabla \cdot (f \vec{U}) = \frac{\partial f}{\partial t} + \frac{\partial}{\partial \vec{r}} (f \cdot \vec{v}) + \frac{\partial}{\partial \vec{v}} \left(f \frac{\vec{F}}{m} \right) = 0 \tag{8}$$

where $\vec{v}$ and $\vec{F}/m$ are dependent on $\vec{r}$ and $\vec{v}$, respectively. Both the conservative form (8) and the advection form (1) of the Vlasov equation are equivalent as one can easily find out by carrying out the partial differentiation in the conservative Vlasov Eq. (8) following the product rule

$$\frac{\partial f}{\partial t} + \vec{v} \cdot \frac{\partial}{\partial \vec{r}} f + \frac{\vec{F}}{m} \cdot \frac{\partial}{\partial \vec{v}} f + f \left\{ \frac{\partial}{\partial \vec{r}} \vec{v} + \frac{\partial}{\partial \vec{v}} \cdot \frac{\vec{F}}{m} \right\} = 0 \tag{9}$$

Since for the Vlasov equation the phase space element is incompressible (the Liouville theorem applies) $\partial \vec{v}/\partial \vec{r} + \partial(\vec{F}/m)/\partial \vec{v} = (\nabla \cdot \vec{U}) = 0$, from Eq. (9) follows that advection and conservative form of the Vlasov equation are indeed equivalent.

Finally, let us provide as another example the relativistic Vlasov-equation in the conservative form:

$$\frac{df_j}{dt} = \frac{\partial f_j}{\partial t} + \frac{\partial}{\partial \vec{r}} \vec{p} f_j + \frac{1}{m_j} \frac{\partial}{\partial \vec{p}} \left(\vec{F}(\vec{E}, \vec{B}, \vec{p}) f_j \right) = 0 \tag{10}$$

where both the momentum $\vec{p}$ and the forces $\vec{F}(\vec{E}, \vec{B}, \vec{p})$ are dependent variables.

3 Numerical Methods

Since the total derivative of the distribution function vanishes, the Vlasov-equation is strictly speaking, non-dissipative and, therefore, entropy conserving, i.e. the consequences of the action of the electromagnetic forces $\vec{F} = e_j(\vec{E} + \frac{1}{c}\vec{v} \times \vec{B})$ is neither dissipated nor otherwise removed from the system. However, the free-streaming character of the evolution of the distribution, arising from the character of the Vlasov-equation, causes an increasingly fine filamentation of the distribution function in the phase space as shown in Fig. 3. The ongoing filamentation creates stronger and stronger phase space gradients, whose inaccurate numerical treatment may lead to oscillations and, finally, to numerical instabilities un-physically disrupting the system.

In PIC-codes the mathematically correct filamentation is smeared out by the shot noise of the finite number of macro-particles, representing the phase space in a discrete way (in contrast to the non-grained character of an ideal collisionless solution). In Vlasov solvers the gradients continue to grow. Their correct treatment is a major issue in the numerical solution of the Vlasov equation.

Since one has to avoid the growth of oscillations, the use of higher order schemes might be counterproductive. Often numerical problems due to the filamentation are treated by introducing artificial dissipation, by smoothing or by filtration. Denavit (1972), e.g., used a periodic smoothing in the phase space while Klimas and Farrel (1994) implemented a filtration technique. Physically these procedures correspond to wave damping after down-cascading the perturbations to small sales.

Undamped non-physical oscillations are often the cause that the newly calculated distribution function become negative. Since the positivity of the distribution function has to be maintained some codes just put newly calculated negative distribution

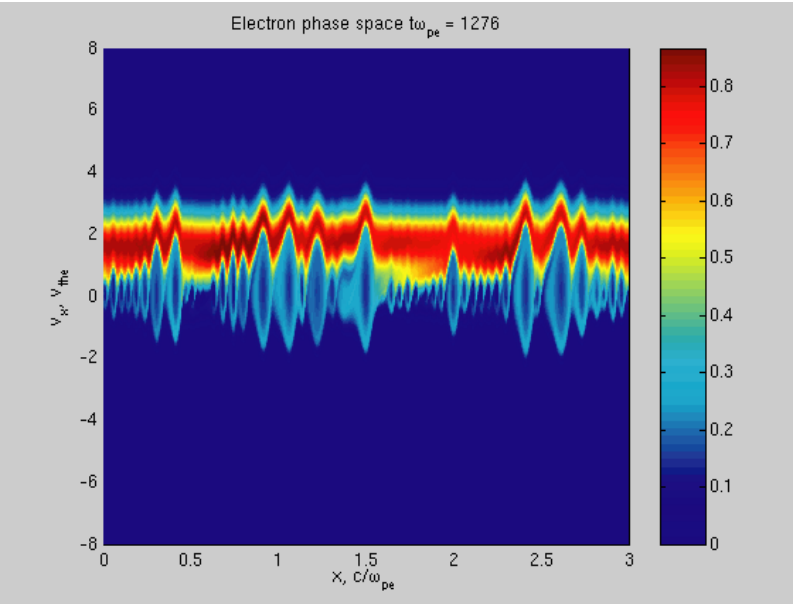

Fig. 1. Filamentation of the electron distribution function obtained by a highly accurate, realistic mass ratio 1D1V conservative Vlasov code simulation of an ion sound instability. From Büchner and Elkina (2006a).

function values to zero. In this way, however, the number of particles and energy are not conserved and the simulation results become unreliable.

The only correct way to maintain positivity is the choice of a sufficiently accurate solution scheme. Lagrange schemes are most accurate. Although corresponding attempts were made in the 1960's ("waterbag" schemes), consequent Lagrange schemes are not well applicable due to the increasing with time complication of the phase space structures, which has to be tracked down.

3.1 Semi-Lagrange methods

Given the above difficulties with fully Lagrangian methods semi-Lagrange schemes have been developed. Such schemes first use the fact that the most accurate way to solve convection (or advection, term $v\delta_r f$) hyperbolic PDE is to use their characteristics, along which the function value (here the distribution function) stays constant. The characteristics of the Vlasov-equation are the particle orbits in response to the selfconsistently calculated electromagnetic forces (this is also used in PIC codes). Although the phase space filamentation inhibits the use of this property to construct a straightforward Lagrange method of solution, semi-Lagrange schemes were successfully implemented to solve low-dimensional problems. In their pioneering work Cheng and Knorr (1976) utilized a semi-Lagrangian solution of the Vlasov-

equation. (Their second ground breaking achievement, time splitting, is discussed below.) The semi-Lagrange approach is most accurate since along the characteristics the distribution function f stays unchanged. To obtain the solution on a spatial and velocity-space Euler-grid, however, one has to extrapolate the time advanced distribution function onto the neighboring Euler-grid- points. This introduces numerical errors (Sonnendrücker *et al.*, 1998). In low-dimensional systems the semi-Lagrange method is very efficient. Applied to higher dimensional problems their efficiency suffers, however, from the difficulties of multidimensional extrapolation. Semi-Lagrange methods are accurate and robust because they use an analytic solution. Their disadvantage is the necessity to carry out interpolations back to the Euler grid making semi-Lagrange schemes numerically increasingly expensive for higher dimensional problems.

The second important step forward in Vlasov coding was another great idea of Cheng and Knorr (1976), whereby the split the advection-type Vlasov-equation (1) into two advection equations, one in real space and one in velocity space. Both equations are solved sequentially by the following stepping algorithm: first one evolves $\delta_t f + v\delta_r f = 0$ for $\Delta t/2$ then one solves the field equation, then one evolves $\delta_t f + F\delta_v f = 0$ for Δt and, finally, one obtains the new function value $\delta_t f + v\delta_r f = 0$ at $t + \Delta t$. Cheng and Knorr (1976) renamed the fractional stepping "time splitting". However, like any non-conservative scheme, the stepping algorithm, which calculates function values at different moments of time, introduces numerical dissipation. Nevertheless, the semi-Lagrangian method with time splitting (see also Cheng, 1977; Gagné and Shoucri, 1977; Shoucri, 1979) for many years has been the most commonly used scheme of space plasma Vlasov code simulations. While the attention of the researchers was focussed on improving the accuracy of semi-Lagrangian advection equation solvers (see, e.g., Horne and Freeman's (2001) McCormac scheme) unfortunately, not much attention has been devoted to the further development of Vlasov-solvers on Eulerian grids.

3.2 Functional expansion (transform) methods

For special applications, transform methods of solving the Vlasov-equation might be useful. Different transform methods are discussed, e.g., by Armstrong *et al.* (1976). A 2D2V Fourier transform solution of the Vlasov-equations was developed by Eliasson (2003). Other functional expansions, like into Hermite polynomials, spherical harmonics, might be appropriate as well (see, e.g. Shebalin, 2001). Expansion methods are very efficient if they can use specific symmetries. In general, however, expansion methods are less recommendable than straightforward Euler schemes. They generally cause difficulties in formulating the boundary conditions. Filamentation calls for the introduction of higher and higher order polynomials. Another difficulty is the transformation in case of decomposition for the sake of parallelization domains. Further, spectral methods suffer from the same problems as higher (>1st)-order unlimited Eulerian schemes - a monotonicity- preserving spectral scheme has yet to be developed.

3.3 Euler methods

In contrast to semi-Lagrangian schemes, Eulerian grid methods omit the extrapolation of the distribution function by directly calculating the function values on the grid, which can be the same as the one, used for calculating the electromagnetic field values or a staggered one. In contrast to functional expansion methods, Eulerian schemes are most flexible concerning the boundary conditions, allowing also open boundaries. A critical discussion of existing Eulerian Vlasov solvers can be found in Arber and Vann (2002).

Since space physics problems are mostly higher dimensional, most accurate schemes are necessary such as conservatively solving the Vlasov-Eq. (8). Appropriate algorithms can make the Eulerian solution of Vlasov-equations in their conservative form as accurate as semi-Lagrangian algorithms (see, e.g., Filbet *et al.*, 2001). From the computational fluid dynamics it is well known that a highly accurate numerical integration of continuity equations arise from the use of flux-corrected transport (FCT) algorithms (e.g., Zalesak, 1979). Boris and Book (1977) successfully applied an FCT scheme to the solution of the Vlasov equation in 1D1V. A finite volume discretization flux-limited transport (FLT) scheme, however, might be the solution of choice. In Elkina and Büchner (2006) we have utilized a finite volume discretization (FVD) using a flux limited transport (FLT) approach taking into account also the diagonal elements to enhance the accuracy.

Let us demonstrate the main steps in such finite volume discretization in 1D1V case $((x, v))$ with a rectangular boundary. Let us start with the integral form Vlasov Eq. (7), which can be rewritten as

$$\frac{\partial}{\partial t}\int_{\Omega} f d\Omega = -\oint_{S(\Omega)} \vec{H}\vec{n} dS \tag{11}$$

The discretization subdomains are defined on a rectangular grid in the (x, v) 1D1V phase space, breaking the simulation domain Ω down into $N_x \times N_v$ non-overlapping subdomains $V_{i,j}$ such that

$$\Omega = \bigcup_{i,j=0}^{N_x \times N_v} V_{i,j} \tag{12}$$

N_x and N_v are the numbers of grid points in the x and v directions. Let us relate the distribution function $f_{i,j}$ to the center of each subdomain $V_{i,j}$ while the fluxes through the subdomain boundaries as depicted in Fig. 4 (shown are the integral fluxes $G = \int_{t,\Delta S} H(f) dS dt$, see Eq. (17), instead of the differential fluxes H). The volume of a subdomain (cell) $V_{i,j}$ is given by $[\Delta x_i \times \Delta v_j] \times [t_n; t_{n+1}]$, where $\Delta x_i = x_{i+1/2} - x_{i-1/2}$ and $\Delta v_j = v_{j+1/2} - v_{j-1/2}$ and the average over the subdomain $V_{i,j}$ distribution function $f_{i,j}$ is given at t_n as

$$\overline{f}^n_{i,j} = \frac{1}{|V_{i,j}|}\int_{V_{i,j}} f(\vec{r}, \vec{v}, t_n) dV \tag{13}$$

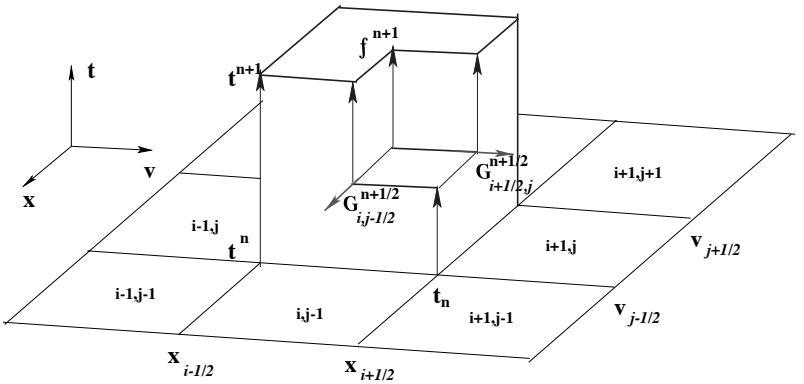

Fig. 2. 1D1V temporal and spatial control volumes (subdomain) for a finite volume discretization, from Elkina and Büchner (2006).

The integral conservative Vlasov equation in its form (11) can now be expressed as

$$\frac{\partial \overline{f}^{n}_{i,j}}{\partial t} = -\frac{1}{|V_{ij}|}\int_{t_n}^{t_{n+1}} \oint_{\partial V_{ij}} \vec{H}_{i,j}\vec{n}_{i,j} dS dt \tag{14}$$

where $\vec{n}_{i,j}$ denotes the outward directed normals of the subdomain (cell) boundary ∂V_{ij}. In our rectangular grid geometry each subdomain V_{ij} is bounded by four perpendicular sides $\Delta S_{i,j,\beta}$ ($\beta = 1-4$). The surface integral in (14) can be replaced by the sum over the fluxes through the four sides:

$$\oint_{\partial V_{i,j}} \vec{H}(f)_{i,j}\vec{n}_{i,j} dS = \sum_{\beta=1}^{4} \int_{\Delta S_{i,j,\beta}} \vec{H}(f)_{i,j}\vec{n}_{i,j,\beta} dS \tag{15}$$

Equations (14) and (15) establish a discrete evolution equation for the mean values of the distribution function $\overline{f}^{n}_{i,j}$. A finite volume method solves directly for the time advanced distribution function value. Hence, the discrete value of the distribution at t_{n+1} can be obtained as (in the following we omit the average-overline, i.e., $\overline{f}_{i,j} \rightarrow f_{i,j}$)

$$f^{n+1}_{i,j} = f^{n}_{i,j} - \frac{\Delta t}{|V_{i,j}|}\sum_{\beta=1}^{4} G^{n+\frac{1}{2}}_{i,j,\beta} \tag{16}$$

In Eq. (16) we expressed the fluxes through the boundary segments $\Delta S_{i,j,\beta}$ by their discrete integral values $G^{n+1/2}_{i,j,\beta}$ which follow from Eqs. (14) and (15) as

$$G_{i,j,\beta}^{n+1/2} = \frac{1}{\Delta t}\int_{t_n}^{t_{n+1}}\int_{\Delta S}\vec{H}(f)\vec{n}_{i,j,\beta}dSdt \tag{17}$$

In order to obtain a second order accurate time discretization we approximate the flux function at the center of each subdomain boundary at half the time step $(n+\frac{1}{2})$. Using the midpoint rule for the time integration one finds

$$G_{i,j,\beta=1,2} = \{G_{i\pm\frac{1}{2},j}\} \quad G_{i,j,\beta=3,4} = \{G_{i,j\pm\frac{1}{2}}\} \tag{18}$$

Each flux through a cell boundary depends on the cell to the left and on the cell to the right:

$$G_{i+\frac{1}{2},j,S} = g(G_{i+\frac{1}{2},j,L}, G_{i+\frac{1}{2},j,R}) \tag{19}$$

The determination of the flux through the subdomain (cell) boundaries $\delta V_{i,j}$ corresponds to the solution of a Riemann problem. At the beginning of each time step the fluxes set up an unsteady Riemann problem at each subdomain (cell) boundary. The solution of the Riemann problem determines the domain of dependence of each subdomain. Due to the causality principle one can approximate the solution at each time step inside the domain of dependence. For this purpose we use the first order Godunov (1959) flux functions

$$G_{i+1/2,j} = U_x^+ f_{i,j} + U_x^- f_{i+1,j} \tag{20}$$

where

$$U_x^+ = \max(U_x, 0) \qquad U_x^- = \min(U_x, 0) \tag{21}$$

to obtain an upwind scheme. A numerical solution of the discrete conservative Vlasov Eq. (16), using first order fluxes defined by Eqs. (20) and (21), would provide a first order scheme with the stability condition given by Colella (1991)

$$\left|v\frac{\Delta t}{\Delta x}\right| + \left|\frac{F}{m}\frac{\Delta t}{\Delta v}\right| \leqq 1 \tag{22}$$

We enhance the accuracy of our scheme to the second order by introducing a more sophisticated approximation of the averaged quantities inside the subdomain using a piecewise-linear approximation based on a Taylor series expansion of the subdomain boundary values for the determination of the fluxes inside the upwind cells. Let us describe the second order approximation taking the calculation of $G_{i+\frac{1}{2},j}$ as an example (all other fluxes are calculated in the same way, just interchange the indices i, j and x, v). We define the left and right side flux function as: $G_{i+\frac{1}{2},j,S} \in (G_{i+\frac{1}{2},j,L}, G_{i+\frac{1}{2},j,R})$ where $G_{i+\frac{1}{2},j}$ is obtained by solving the Riemann problem:

$$G_{i+\frac{1}{2},j} = g(G_{i+\frac{1}{2},j,R}, G_{i+\frac{1}{2},j,L})$$

where:

$$G^{n+\frac{1}{2}}_{i+\frac{1}{2},j,S} = U^{+}_{x} f^{n}_{i,j} + U^{-}_{x} f^{n}_{i+1,j} \pm \frac{\Delta x}{2}\frac{\partial f}{\partial x} + \frac{\Delta t}{2}\frac{\partial f}{\partial t} \tag{23}$$

Substituting $\partial f/\partial t$ using the Vlasov equation (8) one obtains

$$G_{i,j,S} = U^{+}_{x} f^{n}_{i,j} + U^{-}_{x} f^{n}_{i+1,j} \pm \frac{\Delta x}{2}\frac{\partial f}{\partial x} + \frac{\Delta t}{2}\left(\frac{\partial H^{x}}{\partial x} + \frac{\partial H^{v}}{\partial v}\right) \tag{24}$$

and, after some rearrangement, one finds, the second order upwind flux function

$$G_{i+1/2,j,S} = f_{i+k,j} + \left(\sigma_{i+1/2,j} - \frac{\Delta t}{\Delta x} U^{x}_{i+1/2,j}\right) H^{x}_{i+1/2,j} - \frac{\Delta t}{2}\frac{\partial H^{v}}{\partial v} \tag{25}$$

where $\sigma_{i+1/2,j} = \mathrm{sign}(U^{x}_{i+\frac{1}{2},j})$. The first term in expression (25) provides a first order upwind scheme. The middle term provides second order accuracy correction. The third is a transverse propagation term from the diagonally located subdomain.

As it is well known, second order schemes can cause un-physical oscillations which may lead to negative values of the distribution function or even to numerical instabilities. To avoid such instabilities we limit the physical flux $H^{x}_{i+\frac{1}{2},j}$ in the middle, the second (order) term of Eq. (25). The limiter function, that applies directly to the derivatives, is given by

$$H^{x}_{i+1/2,j} = \mathrm{Limiter}\left\{Q^{C}_{i,j}, Q^{R}_{i,j}, Q^{L}_{i,j}\right\} \tag{26}$$

where $Limiter$ is a nonlinear function based on the gradient of the solution. Near steep gradients the flux limitation reduces our method to a first order upwind scheme. The central, right and left derivatives in the *Limiter* function (26) are given by

$$Q^{C}_{i,j} = f_{i+1,j} - f_{i-1,j}, \quad Q^{R}_{i,j} = f_{i+1,j} - f_{i,j} \quad Q^{L}_{i,j} = f_{i,j} - f_{i-1,j}$$

We successfully applied in our simulations the following flux limiter:

$$Limiter\left\{Q^{C}_{i}, Q^{R}_{i}, Q^{L}_{i}\right\} = \begin{cases} \min\left\{\frac{1}{2}|Q^{C}_{i,j}|, 2|Q^{L}_{i,j}|, 2|Q^{R}_{i,j}|\right\} & Q^{R}_{i,j} Q^{L}_{i,j} > 0 \\ 0 \quad \text{otherwise} \end{cases} \tag{27}$$

A limiter in the form (27) satisfies the maximum principle, i.e. it does not introduce new extrema. This guarantees the absolute preservation of a positive (positivity) value of the distribution function.

Let us now consider the transverse propagation term in the expression for discrete integral flux function (25). We approximate it by choosing the Godunov function. If $H^{T}_{i,j+1/2}$ is the solution of the Riemann problem projected along the v-direction with the left and right side expressions:

$$(H^{T}_{i,j+1/2,L}, H^{T}_{i,j+\frac{1}{2},R}) = (U^{v}_{i,j+\frac{1}{2}} f^{n}_{i,j}, U^{v}_{i,j+\frac{1}{2}} f^{n}_{i,j+1}) \tag{28}$$

then the transversal term in Eq. (25) can be written as:

$$\frac{\Delta t}{2}\frac{\partial H^v}{\partial v} = \frac{1}{2}\frac{\Delta t}{\Delta v}\left(H^T_{v,i+k,j+\frac{1}{2}} - H^T_{v,i+k,j-\frac{1}{2}}\right) \tag{29}$$

where $k = 0, \pm 1$ determine of the upwind subdomain.

Finally, after Colella (1991) the stability condition for the second order scheme is given by:

$$\max\left(\left|v\frac{\Delta t}{\Delta x}\right|, \left|\frac{F}{m}\frac{\Delta t}{\Delta v}\right|\right) \leqq 1 \tag{30}$$

Let us discuss the optimum choice of the grid scaling. The maximum possible time step size is determined by the stability condition (30). The corresponding necessary Courant-Friedrich-Levy (CFL) condition is $CFL \leq 1$.

We choose the time step Δt determined in the ($1D1V$) phase space for both electrons and ions plasma species in the whole simulation domain in accordance with:

$$\Delta t = CFL \cdot \min\left[\frac{\Delta x}{\max(v^e_{\max}, v^i_{\max})}, |C_e| \cdot \left(\frac{\Delta v^e}{E^{\max}_x}\right), |C_i| \cdot \left(\frac{\Delta v^i}{E^{\max}_x}\right)\right] \tag{31}$$

where $v^{\max}_e$, $v^{\max}_i$ are the maximum velocities in the simulation box for the plasma species and $E^{\max}_x$ is the maximum electric field. $CFL = 0.8$ is used for all simulation runs presented here.

The necessary condition for grid sampling in real space is the quasi-neutrality condition, which requires a resolution of the Debye length $\lambda_D = v_{te}/\omega_{pe}$, where $v_{te} = \sqrt{T_e/m_e}$ and T_e is the electron temperature in energy units:

$$\Delta x < \lambda_D \tag{32}$$

The choice of the number of spatial and velocity space Eulerian grid points for the numerical integration of the discrete solution determines the smallest phase space filaments, which can be resolved. The choice of Δv determines, therefore, the smoothing, i.e. the minimum numerical dissipation in the system. The actual choice of the velocity space resolution, always depends on the problem studied. Δv_i, for example, should be much smaller than any physically relevant velocity space granulation.

While the Vlasov equation itself is non-dissipative (Hamiltonian), (numerical) dissipation arises due to its discrete representation on a Eulerian grid. Once the filaments reach the mesh-size scale, any finer filamentation becomes smoothed away numerically. At the same time large scale structures are unaffected. The evolution on the fine scales can be estimated from the solution of the free-streaming Vlasov equation, Fourier transformed in real space ($f(v, x, t) \rightarrow f(v, k, t)$)

$$f(v, k, t) = f(v, k, 0)e^{i\eta v} \tag{33}$$

When $\eta = kt$ reaches the inverse of Δv one can no longer follow the further filamentation of f and the information is lost. This takes place especially within

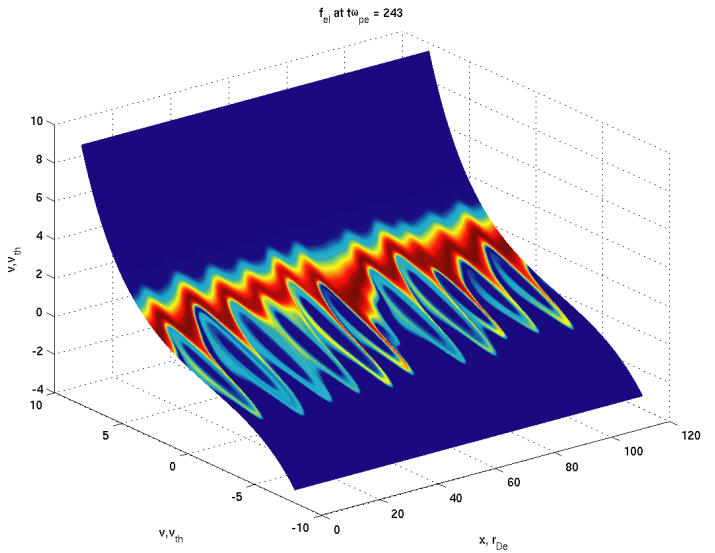

Fig. 3. Filamented electron phase space obtained with $Str = 2$ on a stretched 512×512 grid (for a triggered ion-acoustic instability—see Section 5.1). From Büchner and Elkina (2006a).

$\Delta = \eta^{-1} = 1/kt$ of the resonance velocity, i.e. Δ is the characteristic width of the resonance. Only particles within Δ of the resonance velocity experience a significant contribution to or deduction of its kinetic energy (O'Neil, 1965). The linear stage ends at saturation. Single-mode systems saturate when the electric field reaches an amplitude $E_{\rm sat}$ for which the trapping frequency is of the order of the linear growth rate γ of a given instability

$$\omega_t = \sqrt{\frac{eE_{\rm sat}k}{m_e}} \simeq \gamma$$

which can be derived solving the linear dispersion relation. The characteristic saturation time may be estimated for an initial perturbation δE_0, since $E_{\rm sat} = \delta E_0 e^{\gamma t_{\rm sat}}$, as

$$t_{\rm sat} = \frac{1}{\gamma} \ln\left(\frac{\gamma^2 m}{e\delta E_0}\right)$$

Thus the characteristic width of the resonance region at saturation may be estimated as

$$\Delta = \frac{1}{kt_{\rm sat}} = \frac{\gamma}{k \ln(\gamma^2 m/e\delta E_0)} \tag{34}$$

which should be resolved by the velocity space grid:

$$\Delta v \ll \Delta \tag{35}$$

A way to decrease the numerical dissipation without increasing the total number of grid cells is the use of a non-uniform grid stretching which refines the mesh at places where the finest filaments are expected, i.e. near resonances, while stretching it away from the resonances. This can be done when the main resonance region is known. In our example this is the ion-acoustic wave velocity, the ion-sound speed $c_{ia} = \sqrt{T_e/M_i}$. Consequently we applied a stretching function

$$V_i^{\mathrm{str}} = v^{\max} \frac{\sinh\left((v_i - v_{\mathrm{res}})\mathrm{Str}/v^{\max}\right)}{\sinh(\mathrm{Str})} \tag{36}$$

where Str is the stretching factor, V_i^{str} is the velocity value on the non-uniform grid and v_i the velocity value on the original, equally spaced grid, $v_{\mathrm{res}} = c_{ia}$ and $v^{\max}$ is the maximum velocity considered. We perform simulations with the non-equidistant distribution of velocity space grid points V_i^{str} which concentrate near the resonance velocity for simulation of the ion-acoustic turbulence (see Section 5.1). Figure 3 depicts the electron distribution function at an instant of time on the nonuniformly stretched grid near the resonance velocity space grid surface.

4 Boundary Conditions

Vlasov-codes require, in addition to the boundary conditions in the real space, bondary conditions in the velocity space as well.

The simplest choice of a boundary condition is maintaining the initial distribution function values at the velocity space boundaries. This approach might, however, cause problems because any acceleration (i.e. redistribution toward the boundaries of the velocity space) accumulates plasma near the velocity space boundary causing growing gradients. This is especially crucial in multidimensional applications where the velocity space is technically limited to only a few thermal velocities. The accumulation results in a non-physical charge separation and electric field generation which finally causes the field solver explode. To avoid such problems one can introduce an appropriate, not too small, not too large, amount of dissipation $\partial f/\partial t = \nu \partial^n f/\partial v^n$ with $n = 4, 6, 8$ near the boundary. A more sophisticated approach is the removal of short wavelength oscillations by Fourier filtering of large-k modes. The latter, and to some extent also the former method, simulate what physically happens in the real world: after cascading energy towards smaller and smaller scales, microscopic dissipation removes the excess energy avoiding further filamentation. Another way is to change the order of the solver from higher, say a fourth order central scheme, to a lower order scheme when approaching the velocity space boundary setting at the very boundary df/dv to zero.

Another possibility is, as for the calculation of the spatial derivatives, the introduction of ghost grid-cells or ghost zones for the velocity-space boundaries. Ghost zones are created by surrounding the boundary with additional grid cells, used to

buffer appropriate neighboring values of data. The ghost boundary can have a width greater than 1. For example, for a computation of new values for a boundary grid point using values from 2 grid points, the ghost boundary should have a width 2.

For a finite volume discretization as discussed in Section 3.3 one sees from the r.h.s. of Eq. (7) that the flows of the distribution function with the velocity $\vec{U}$ through the boundaries of the simulation domain Ω have to be given. One should distinguish two parts of the boundary $S(\Omega)$, an inflow and an outflow part given by

- inflow: $\Gamma^- = \{\vec{r}, \vec{v} \in S | U_n < 0\}$
- outflow: $\Gamma^+ = \{\vec{r}, \vec{v} \in S | U_n > 0\}$

Figure 4 provides an example of an open boundary system. The schematics shows the boundary conditions for an electron (f_e, solid line) and an ion distribution (f_i, dotted line) at the two inflow boundaries Γ^-. The open outflow boundaries Γ^+ are indicated by flow arrows.

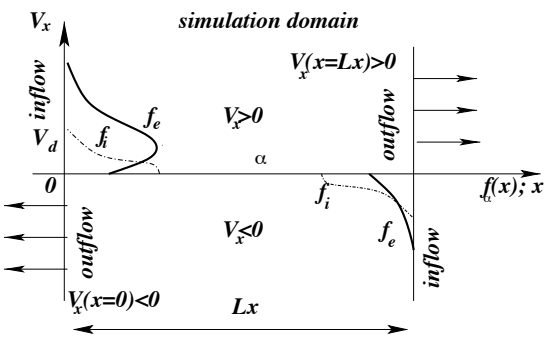

Fig. 4. Schematics of boundary conditions f_e (solid line) depicts an electron—and f_i (dotted line) an ion distribution function at the two inflow boundaries Γ^-. The outflow boundaries Γ^+ are kept open, indicated by flow arrows, as implemented by Büchner and Elkina (2006b).

5 Vlasov Code Applications in Space Physics

A common space physics application of Vlasov-codes is the simulation of electrostatic waves. Klimas and Farrel (1994), e.g., used a 1D1V Vlasov-code to simulate the electron acceleration induced by beam instabilities in the Earth's foreshock region. Let us consider here different important cases of ion-acoustic instabilities in space plasmas.

5.1 Triggered ion-acoustic instability

For an electrostatic perturbation the ion-acoustic (IA) instability can be considered in one spatial (x) and one velocity space dimension ($v_x \rightarrow v$), i.e. in 1D1V. In the simplest case the instability causes just electrostatic oscillations in the x-direction ($E_x \rightarrow < E > + E$). In this limit the Vlasov-Maxwell system of field equations can be reduced to a set of two one-dimensional Vlasov and a one-dimensional Ampère

equation for the perturbed current ($J_x \rightarrow < J > + J$), to which an external current $J_{\text{ext}} =< J >$ is added. This external, average current balances the average magnetic field ($\nabla \times < \vec{B} >=< J >= J_{\text{ext}}$) such that $\partial/\partial t < E >= 0$ (Horne and Freeman, 2001).

$$\frac{\partial f_\alpha}{\partial t} + v\frac{\partial f_\alpha}{\partial x} + \frac{1}{C_\alpha}\frac{\partial f_\alpha}{\partial v} = 0 \qquad \frac{\partial E}{\partial t} = -J + J_{\text{ext}} \tag{37}$$

To complete the code one has to formulate a Vlasov–solver discretization of the electrostatic Ampère equation (37). Since the electric field enters the flux $G^{n+\frac{1}{2}}_{i,j\pm\frac{1}{2}}$ it is appropriate to determine E also at each half-time step $t^{n+1/2}$. Hence, $E_{i,j\pm 1/2}$ should be calculated as

$$E^{n+\frac{1}{2}}_{i,j\pm\frac{1}{2}} = E^{n-\frac{1}{2}}_{i,j\pm\frac{1}{2}} - \Delta t \cdot J^n_{i,j\pm\frac{1}{2}} \tag{38}$$

while the current $J^n_{i,j\pm\frac{1}{2}}$ should be calculated synchronously with the advancement of the distribution function. Now one has to solve Eq. (38) together with the discretized Vlasov equation, e.g. as derived in Section 3. In order to investigate the stability of a plasma system by a practically noiseless Vlasov-code one has to start the system with appropriate initial conditions. First of all, one needs initial electron and ion distribution functions. To introduce free energy into the system, let us assume that the electrons drift against a background of a resting ion distribution. Also, in order to overcome the lack of a low-level background electric field in a noiseless system, let us modulate the electron distribution in space to trigger a spectrum of waves:

$$f_e = (1 + a^e(x))\sqrt{\frac{1}{\pi \cdot v_{te}^2}}\exp\left(-\frac{(v_e - v_{de})^2}{2v_{te}^2}\right) \tag{39}$$

$$f_i = \sqrt{\frac{1}{\pi \cdot v_{ti}^2}}\exp\left(-\frac{v_i^2}{2v_{ti}^2}\right)$$

where $v_{t\alpha} = \sqrt{T_\alpha/m_\alpha}$ (T_α is the temperature) are the electron and ion thermal velocities, respectively, and v_{de} is the drift speed of the electrons as suggested by Arber and Vann (2002). We used for the perturbation of the initial electron distribution function $a^e(x)$ the form function

$$\begin{aligned} a^e(x) = 0.01(&\sin(x) + \sin(0.5x) + \sin(0.15x) + \sin(0.2x) \\ &+ \cos(0.25x) + \cos(0.3x) + \cos(0.35x)) \end{aligned} \tag{40}$$

Note that both distribution functions (40) are normalized to the total number of particles (N_α), i.e.

$$\int_{-\infty}^{\infty} f_\alpha dv_\alpha = 1 \tag{41}$$

Let us discuss the results of runs carried out for the following physical parameters:

$$C_i = M_i/m_e = 1000; \quad T_i = 0.5T_e; \quad T_e = 10 \quad eV, \quad v_{de} = 2v_{te} \tag{42}$$

Appropriate parameters of the numerical scheme are, e.g.,

$$L_x = 0.1\frac{c}{\omega_{pe}} \approx 120\lambda_D; \quad v_e^{\max} = 8v_{te} \quad v_i^{\max} = 8v_{ti} \tag{43}$$

Let us use periodic boundary conditions in real space and a Dirichlet boundary condition in the velocity space maintaining f constant at the velocity space boundary as determined by initial condition. For a run with $N_x = 512$ x $N_v = 512$ the resulting

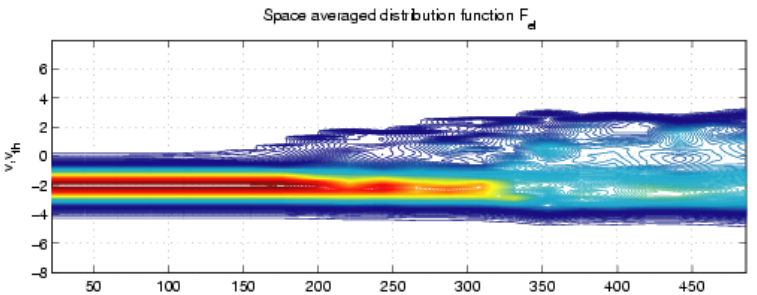

Fig. 5. Time evolution of the spatially averaged electron distribution function $f_e = F_e$ in the course of a triggered ion-acoustic instability, $N_x \times N_v = 512 \times 512$. From Elkina and Büchner (2006).

evolution of the electron distribution function, spatially averaged over the whole spatial simulation domain L_x, is shown in Fig. 5. As can see in Fig. 5 for the physical parameters given by Eq. (42) the ion-acoustic instability leads to a considerable deformation of the drift-electron distribution after about $t\omega_{pe} = 150$. The reason is that the IA waves obtained energy from the drifting electron distribution and transferred it to the ions via resonant interaction of the fluctuating electric field with the particles. This leads to a deformation of the distribution functions of the electrons as shown in Fig. 5 and of the ions as well. Finally, at about $t\omega_{pe} = 200$ a transition takes place from a quasi-linear to a strongly non-linear wave-particle interaction.

5.2 Spontaneous ion-acoustic instability

Let us now consider the problem of a spontaneously arising IA instability in a current carrying plasma. A spontaneous ion-acoustic instability is excited only if $v_{de} > v_{\text{crit}}$. The value of v_{crit} can be determined by solving the linear dispersion relation. This time, however, instead of imposing an electron drift as in the case of the triggered ion acoustic instability considered in Section 5.1, we apply a constant electric field to an initially unperturbed system of resting Maxwellian distributed electrons and ions. Since a Vlasov code is noiseless we have to add random fluctuations

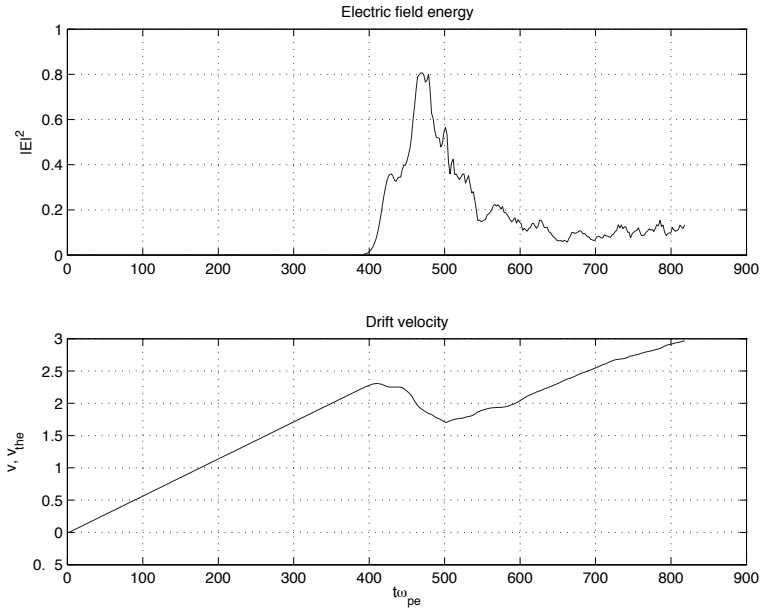

Fig. 6. Time evolution of the energy of the electric field fluctuations (upper panel) and of the average particle drift (current) velocity. From Elkina and Büchner (2006).

δf_α, so that the initial distribution will be given by

$$f_\alpha = \sqrt{\frac{1}{\pi \cdot v_{t\alpha}^2}} \exp\left(-\frac{(v_\alpha)^2}{v_{t\alpha}^2}\right) \cdot \left(1 + \frac{\delta f_\alpha}{f_\alpha}\right) \tag{44}$$

In our simulations we have chosen a fluctuation amplitude at the thermal noise level. Initially, both electrons and ions are accelerated in an external electric field E_0^{ext}. When their relative drift reaches the critical speed v_{crit}, the plasma becomes unstable and ion-acoustic waves are generated. Omura *et al*. (2002) investigated this problem by means of their one-dimensional PIC code KEMPO1. For better comparison of the results we use the same ratio of ion to electron thermal velocities and apply the same external electric field strength:

$$v_{ti} = 0.0625\, v_{te}; \qquad E_0^{\text{ext}} = 0.01$$

The other simulation parameters were

$$C_i = M_i/m_e = 100; \qquad T_i = 0.4T_e; \qquad T_e = 10eV$$

while the parameters of the numerical scheme were

$$L_x = c/\omega_{pe} \approx 460\lambda_D \quad v_e^{\max} = 12v_{te} \quad v_i^{\max} = 12v_{ti}$$

The grid resolution of this simulation was $N_x \times N_v = 256 \times 256$.

As one can see in the upper panel of Fig. 6, after about $t\omega_{pe} = 400$, electric field fluctuations start to grow strongly The lower panel of Fig. 6 shows that the instability starts as soon as the drift velocity reaches $v_{\rm crit} = 2.3v_{te}$. After $t\omega_{pe} = 400$ and until $t\omega_{pe} = 500$ the strongly nonlinear wave-particle resonant interaction reduces the drift speed (Fig. 6, lower panel). Then the resonance condition is not fulfilled any more and the electric field fluctuation energy decreases again, which allows the drift to increase further. Figure 7 depicts the evolution of the spatially averaged electron distribution showing the quasi- and non-linear formation of a plateau in the electron distribution function.

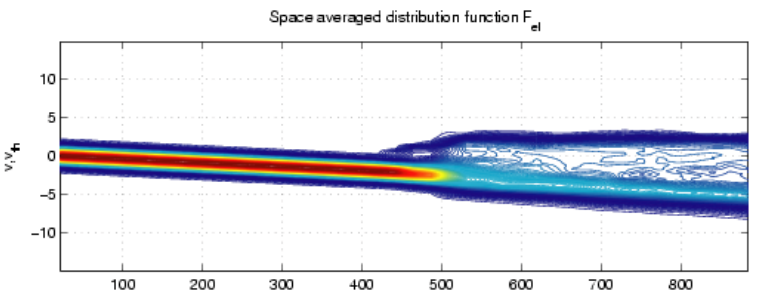

Fig. 7. Evolution of the spatially averaged electron distribution function $f_e = F_e$ in the course of the development of a spontaneous ion-acoustic instability, $N_x \times N_v = 256 \times 256$. From Büchner and Elkina (2006a).

5.3 Formation of double layers

The formation of electrostatic double layers of ion-acoustic waves has been investigated starting with a Buneman instability (de Groot *et al.*, 1977; Sigov, 1982) but for space plasma applications the ion-acoustic case might be of interest as well, although usually $T_e \approx T_i$ instead of the usually assumed hot electron case $T_e \gg T_i$. For the latter, a Vlasov simulation of the formation double layers was carried out by Chanteur (1984) for $T_e = 20T_i$, as reported in the Proceedings of the First International Conference on Space Plasma Simulation, held in 1982 in Kyoto. In space plasmas, where the ion temperature often even exceeds the electron temperature, ion-acoustic waves and double layers are excited in a different regime. In contrast to the two applications discussed in Sections 5.1 and 5.2 it is, however, necessary to continue the energy supply which cannot be done by using periodic boundary conditions. Applying open boundary condition as discussed in Section 4, however, leads to the formation of double layers as shown in (Büchner and Elkina, 2006b).

5.4 LHD/Sausage/kink/reconnection instabilities

Recently, Vlasov-codes have been used also for solving multi-dimensional space physics problems (see, e.g., Wiegelmann and Büchner, 2001). Using a 2D3V Vlasov-code Silin and Büchner (2003) described, e.g., the nonlinear triggering of kinetic kink

and sausage mode instabilities of thin current sheets by linearly unstable lower hybrid drift waves both in antiparallel and in guided (non-antiparallel sheared) magnetic fields. Using a 3D3V version of the code, Silin and Büchner (2005) obtained the triggering of three-dimensional kinetic reconnection by the coupling of the lower hybrid drift instability at the edges of a thin current sheet to reconnection. Note, however that these multi-dimensional Vlasov-code results were obtained for very small artificial mass ratios of about $M_i/m_e = 25$.

5.5 Anomalous resistivity

Another important application of Vlasov codes in space physics is the investigation of the anomalous resistivity of collisionless plasmas (Büchner and Daughton, 2005). Watt *et al.* (2002) used, e.g., a 1D1V Vlasov-Amperé code developed by Horne and Freemann (2001) to investigate the anomalous resistivity due to an ion-acoustic instability driven by a shifted electron Maxwellian distribution in a one-dimensional, periodic boundary system for an artificially small electron- to ion mass ratio, but for the typical for space physics problem situation where the ion temperature is not much less than the electron temperature as usually considered to drive IA waves unstable. Similar ion and electron temperatures require huge electron drift velocities $u_{de} > v_{te} = \sqrt{2k_B T_e/m_e} \gg c_{ia} = \sqrt{k_B T_e/M_i}$ to excite an IA instability (see, e.g., Gary, 1993). For an artificial mass ratio of $M_i/m_e = 25$ Watt *et al.* (2002) obtained resistivity values exceeding the quasi-linear estimate by up to five orders of magnitude. Petkaki *et al.* (2003) extended this study to investigate the influence of Lorentzian distribution functions with small κ values, i.e. for tails enhanced above the Maxwellian distribution. They confirmed a slight enhancement of the linear growth rate obtained by Meng (1992). The anomalous resistivity obtained by these calculations, exceeded by three to five orders the quasi-linear prediction. These results seem to be, however, either an artifact of the low mass ratio or of the method, used. After all these calculations were carried out for an artificially low mass ratio of $M_i/m_e = 25$ Hellinger *et al.* (2004) used a 1D1V Vlasov-code, again with periodic boundary conditions, but based on a Fourier-transform solver of the Poisson equation (Fijalkow, 1999). These simulations did not confirm the results of Watt *et al.* (2002) and Petkaki (2003) when simulating close to realistic mass ratio $M_i/m_e = 1800$. Instead, they found an enhancement of the anomalous resistivity by just an order of magnitude above the quasi-linear prediction, i.e. much smaller than the one previously obtained for the mass ratio $M_i/m_e = 25$. Büchner and Elkina (2006a,b) revisited the anomalous resistivity caused by an ion acoustic instability using a conservative code as described above in Section 3.3. The calculations for periodic boundary conditions (Büchner and Elkina, 2006a) confirmed the findings of Hellinger *et al.*, 2004, while new results were obtained in the case of open boundary conditions and continuous energy supply (Büchner and Elkina, 2006b). In this case, in fact, electrostatic double layers form which determine the total anomalous resistivity (cf. Section 5.3. Using a multidimensional (2D3V) Vlasov code Silin, I., J. Büchner, and A. Vaivads (2005) obtained an estimate for the anomalous resistivity also for the nonlinear stage of the evolution of a lower hybrid drift instability at the edges of thin current sheets. Note, however that these multi-dimensional Vlasov-code

results were obtained for very small artificial mass ratios of about $M_i/m_e = 25$ so they have to be verified by realistic mass ratio simulations.

6 Summary and Outlook

There are, in principal, two ways to solve collisionless plasma problems numerically—the PIC (Particle In Cell) approach and the direct solution of the Vlasov equation by so called Vlasov codes. While technically simpler to implement and to run, PIC codes include and even exaggerate the course-graininess of a plasma by clustering a large number of real particles into artificially large and heavy macro-particles. Vlasov-codes directly address the free flowing character of the distribution without adding artificial noise. Hence, Vlasov codes enable to accurately describe all the fine phase space effects arising, e.g, near resonances, which are smeared out by noisy PIC-codes. Also from the point of view of the numerical effort Vlasov codes successfully compete with PIC codes, if the same requirements concerning noise and phase space resolution are applied. Indeed, the requirements in terms of spatial resolution of the Maxwell-(field) and particle (equation of motion) / plasma (Vlasov)—equation solvers are comparable, in both approaches the mesh size should be of the order of a Debye length λ_D. To compare the numerical expense of PIC and Vlasov codes in reconstructing the velocity space, let us assume that the calculation of the distribution function value in one grid point in velocity space is equally expensive in CPU as well as in memory requirement (Bertrand, 2005). Then, in a PIC code one has to calculate $N_{PIC} = n_m L^D$ of such elementary operations (particle motions) per time step (L is the length per dimension and D the spatial dimension = 1, 2 or 3). A Vlasov code evaluates the distribution functions at $N_v^{D_v}$ grid points in velocity space in $D_v = 1$, 2 or 3 dimensions for each spatial grid point, i.e. $(L/\Delta x)^D$ times, where Δx is the grid-distance in configurational space. The latter must be taken as the order of the Debye length, i.e. $\Delta x \approx \lambda_D$. Hence, the ratio of the number of elementary operations per time step of a Vlasov code over the corresponding number for a PIC code can be, therefore, estimated as

$$\frac{\text{VLASOVops}}{\text{PICops}} = \frac{N_v^{D_v}}{n_m \lambda_D^D} \tag{45}$$

Expression (45) quantifies, what has been verbally expressed earlier in this tutorial. A PIC code recovers and even overestimates the graininess of the plasma by considering macro-particles instead of a continuously flowing distribution function. An increase of the effective plasma parameter $n_m \lambda_D^D$ calculated for the density of the macro-particles n_m, the denominator of expression (45) toward the real plasma parameter of the order of 10^{10} would make the ratio (45) vanish for practically all numbers of velocity space grids N_v. Thus the advantage of the Vlasov code in appropriately describing a collisionless plasma is obvious. Note that $n_m \lambda_D^D$ is nothing other than the well known "number of particles-per-cell" parameter. Or, consider the other way around. Usually, as a "rule of the thumb", PIC codes use about $n_m \lambda_D^D = 100$ particles per cell in order to recover at least some of the properties of collisionless plasmas. The same numerical effort as for a PIC code with 100 particles per cell,

i.e. VLASOVops/PICops = 1, corresponds to running a code with a velocity space resolution of $N_v^{D_v} = 100$. In one-dimensional in velocity space systems this would correspond to a velocity space resolution of $N_v = 100$ grid points, which is very good. Hence, in one velocity space dimension the numerical effort of a Vlasov code is smaller than that of a comparable PIC code. In two velocity space dimensions a Vlasov code would be run with the same numerical effort if $N_v = 10$, bt this would be too coarse. As a rule of a thumb one needs about $N_v = 20$. In 2V (or 2P) this would correspond to a numerical effort of 400 particles-per-cell PIC code. This makes Vlasov codes comparable in numerical effort to PIC codes in 2V as well. By the same arguments the numerical effort of a three-dimensional in velocity space Vlasov code with $N_v = 20$ would compare to a PIC code with 8000 particles per cell. But, remember, these estimates were obtained by comparing a noiseless Vlasov code with a noisy PIC code, whose noise for 100 particles per cell exceeds the thermal noise of space plasmas $\sqrt{n_o \lambda_D^3}/100 \approx 10^4$ times in case of a PIC-code simulation with 100 macro-particles per cell: a reduction of the PIC code noise to the thermal fluctuation level would mean for a space plasma with, typically, $\lambda_D \approx 100$ m and a number density of 10^6 m^{-3} an additional factor of $\sqrt{10^{10}} = 10^5$ (the square root arises from the shot-noise statistics) in the denominator of Eq. (45). To achieve such a noise level would then favor a Vlasov code. As a result one should understand that the often quoted "numerical efficiency of PIC codes" compared to Vlasov codes is due to accepting with the large noise level of PIC codes, which exceeds the thermal noise level in typical space plasmas in case of 100 macro-particles per cell by many orders of magnitude. With the development of modern parallel computer hardware the use of Vlasov-codes instead of PIC codes has become realistic for problems where the large noise of PIC codes is important. The main caveat of Vlasov codes is the necessity to solve a free-floating advection-type partial differential equation with a vanishing right hand side. The lack of an explicit particle collision term, a consequence of the dominance of collective phenomena above binary interactions in collisionless plasmas, causes an unlimited phase space filamentation down to smallest scales. This filamentation has to be treated numerically in an appropriate way. Traditionally semi-Lagrangian splitting schemes are the most used Vlasov equation solvers. For special applications functional expansion (transform) methods might be useful as well. Eulerian grid based schemes are especially accurate and adjustable to any geometry and boundary situation, if combined with a conservative finite volume discretization scheme, as presented in this tutorial. A next step in improving the efficiency of Vlasov codes will be the implementation of adaptive grid methods (AGMs) which will enable an enhancement of the resolution near resonance velocities (momenta) or near other crucial sites in velocity space, e.g., where particles are accelerated. At the same time AGMs can reduce the number of grid points in "inactive" velocity space regions as well. Finally, with increasing computing power it will become possible to avoid having to deal with the high noise levels and the exaggeration of the course-graininess of collisionless space plasmas re-introduced by the consideration of macro-particles in PIC codes. Along this line Vlasov codes are the most powerful and accurate tools

for correctly describing collisionless space plasma phenomena. Already now Vlasov codes are the method of choice in one and two velocity space dimensions if noise is crucial and a fine resolution of phase space is necessary. For higher (two- and three-) velocity space dimensions, adaptive grid methods will have to be developed to increase the numerical efficiency of Vlasov codes.

Acknowledgments. The author gratefully acknowledges discussions with P. Bertrand, N. Elkina, F. Jenko, I. Silin, R. Sydora, Th. Wiegelmann and thanks the referee for his/her comments.

References

Arber, T. D. and R. G. Vann, A critical comparison of Eulerian-grid-based Vlasov solvers, *J. Comput. Phys.*, **180**, 339–357, 2002.

Armstrong, T. P., R. C. Harding, G. Knorr, and D. Montgomery, Solution of Vlasov's equation by transform methods, in *Methods of Computational Physics, vol. 9*, edited by B. Alder, S. Fernbach, M. Rotenberg, Academic Press, New York, 29 pp., 1970.

Bertrand, P., Vlasov code applications, in *Prof. of ISSS-7*, Kyoto, Japan, March 2005.

Birdsall, C. K. and A. B. Langdon, *Plasma Physics via Computer Simulation*, McGraw-Hill, New York, 1985.

Boris, J. P. and D. L. Book, Solution of continuity equations by the method of flux-corrected transport, in *Controlled Fusion, Methods in Computational Physics*, Vol. 16, Academic Press, New York and London, pp. 85–129, 1976.

Büchner, J., Three-dimensional magnetic reconnection in astrophysical plasmas—kinetic approach, *Astroph. Space Sci.*, **264**, 25–42, 1999. (DOI:10.1023/A:1002451401635)

Büchner, J. and W. Daughton, LHD instability in thin current sheets, in *Reconnection of Magnetic Fields: MHD and Collisionless Theory and Observations*, edited by J. Birn and E. R. Priest, Cambridge University press., 2006.

Büchner, J. and N. Elkina, Vlasov code simulation of anomalous resistivity, *Space Sci. Rev.*, **121**, No. 1-4, 237–252, 2006a. (DOI:10.1007/s11214-006-6542-6)

Büchner, J. and N. Elkina, Anomalous resistivity of current-driven isothermal plasmas due to phase space structuring, *Phys. Plasmas*, **13**, 082304-1–082304-9, 2006b. (DOI:10.1063/1.2209611)

Chanteur, G., Vlasov simulations of ion acoustic double layers, in *Computer simulation of Space Plasmas*, edited by H. Matsumoto and T. Sato, Terra Scientific Publishing Company, Tokyo, Japan, pp. 279–301, 1984.

Cheng, C. Z., The integration of the Vlasov-equation for a magnetized plasma, *J. Comput. Phys.*, **24**, 348, 1977.

Cheng, C. Z. and G. Knorr, The integration of the Vlasov-equation in configuration space, *J. Comput. Phys.*, **22**, 330–351, 1976.

Colella, P., Multidimensional upwind methods for hyperbolic conservation law, *J. Comput. Phys.*, **87**, 171–200, 1991.

De Groot, J. S., C. ABrnes, A. E. Walstead, and O. Buneman, Localised structures and anomalous DC resistivity, *Phys. Rev. Lett.*, **38**, 1283–1286, 1977.

Denavit, J., Numerical simulation of plasmas with periodic smoothing in phase space, *J. Comput. Phys.*, **9**, 75–98, 1972.

Eliasson, B., Numerical modelling the Fourier transformed two-dimensional Vlasov-Maxwell system, *J. Comput. Phys.*, **190**, 501–522, 2003.

Elkina, N. and J. Büchner, A new conservative unsplit method for the solution of the Vlasov equation, *J. Comput. Phys.*, **213**(2), 862–875, 2006. (DOI:10.1016/j.jcp.2005.09.023)

Fijalkow, E., Numerical solution of the Vlasov-equation: the 1D code, *Comput. Phys. Comm.*, **116**, 329–335, 1999.

Filbet, F., E. Sonnendrücker, and N. Bertrand, Conservative numerical schemes for the Vlasov equation, *J. Comput. Phys.*, **172**, 166–187, 2001.

Gagné, R. and M. Shoucri, A splitting scheme for the numerical solution of a one-dimensional Vlasov-equation, *J. Comput. Phys.*, **24**, 445, 1977.

Gary, S. P., *Theory of Space Plasma Microinstabilities*, Cambridge University Press, Cambridge, UK, pp. 34–38, 1993.

Godunov, S. K., Finite difference method for the computation of *Math. Sb.*, **7**, 271–306, 1959.

Hellinger, P., P. Trávnícek, and J. D. Menietti, Effective collision frequency due to ion-acoustic instability: Theory and simulations, *Geophys. Res. Lett.*, **31**, L10806, 2004.

Horne, R. B. and M. P. Freeman, A new code for electrostatic simulation by numerical integration of the Vlasov and Ampere equations using MacCormack's method, *J. Comput. Phys.*, **171**, 182–200, 2001.

Klimas, A. J. and W. M. Farrel, A splitting algorithm for Vlasov simulation with filamentation filtration, *J. Comput. Physics*, **110**, 150–163, 1994.

Mangeney, A., F. Califano, C. Cavazzoni, and P. Travnicek, A numerical scheme for the integration of the Vlasov–Maxwell system of equations, *J. Comput. Phys.*, **179**, 495–538, 2002.

Meng, Z., R. M. Thorne, and D. Summers, Ion-acoustic instability driven by drifting electrons in a generalized Lorentzian distribution, *J. Plasma Phys.*, **47**, 445–464, 1992.

Omura, Y., W. J. Heikkila, T. Umeda, K. Ninomiya, and H. Matsumoto, Particle simulation of response to an applied electric field parallel to magnetic field lines, *J. Geophys. Res.*, **108**(A5), 1197, 2003.

O'Neil, T., Collisionless damping of nonlinear plasma oscillations, *Phys. Fluids*, **8**(12), 2255–2262, 1965.

Petkaki, P., C. E. Watt, R. B. Horne, and M. P. Freeman, Anomalous resistivity in non-Maxwellian plasmas, *J. Geophys. Res.*, **108**, 1442–1453, 2003.

Shebalin, J., A spectral algorithm for solving the relativistic Vlasov-Maxwell equations, *preprint NASA/TP-2001-210195*, 19 pages, 2001.

Sigov, Yu. S., Computer simulation of plasma turbulence in open systems, *Physica Scripta*, **2**(2), 367, 1982.

Silin, I. and J. Büchner, Nonlinear instability of thin current sheets in antiparallel and guided magnetic fields, *Phys. Plasmas*, **10**, **9**, 3561–3570, 2003. (DOI:10.1063/1.1599357)

Silin, I. and J. Büchner, Small-scale reconnection due to lower-hybrid drift instability in current sheets with sheared fields, *Phys. Plasmas*, **12**, 012320 (8 pages), 2005. (DOI:10.1063/1.1830015)

Silin, I., J. Büchner, and A. Vaivads, Anomalous resistivity due to nonlinear lower-hybrid drift waves, *Phys. Plasmas*, **12**, 062902 (8 pages), 2005. (DOI:10.1063/1.1927096)

Shoucri, M., Numerical solution of the two-dimensional Vlasov-equation, *IEEE Trans. Plasma Sci.*, **PS7**, 69, 1979.

Sonnendrücker, E., J. Roche, P. Bertrand, and A. Ghizzo, The semi-Lagrange method for the numerical resolution of Vlasov equations, *J. Comput. Phys.*, **149**, 201, 1998.

Vlasov, A. A., O vibrazionnych swoistwach elektronnowo gasa, *J. Exp. Theoret. Phys.*, **8**, 291, 1938 (in Russian).

Watt, C. E., R. B. Horne, and M. P. Freeman, Ion-acoustic resistivity in plasmas with similar ion and electron temperatures, *Geophys. Res. Lett.*, **29**, 1002, 2002.

Wiegelmann, T. and J. Büchner, Evolution of magnetic helicity in the course of kinetic magnetic reconnection, *Nonlin. Proc. Geophys.*, **8**, 127–140, 2001.

Yee, K. S., Numerical solution of initial boundary value problems involving Maxwell's equations in isotropic media, *IEEE Trans. Electromagn. Compat.*, **AP-14**, 302–307, 1966.

Zalesak, S. T., Fully multidimensional flux-corrected transport algorithms for fluids, *J. Comp. Phys.*, **31**, 335–362, 1979.